

A single nanotrench in a palladium microwire for hydrogen detection

T Kiefer¹, F Favier², O Vazquez-Mena¹, G Villanueva¹ and J Brugger¹

¹ Microsystems Laboratory, Station 17, École Polytechnique Fédérale de Lausanne (EPFL), Lausanne, 1015, Switzerland

² ICG-AIME, UMR 5253 CNRS Université Montpellier 2, cc015, Montpellier cedex 5, 34095, France

E-mail: thomas.kiefer@epfl.ch

Received 12 November 2007, in final form 8 January 2008

Published 20 February 2008

Online at stacks.iop.org/Nano/19/125502

Abstract

The hydrogen sensing characteristics of a single nanotrench fabricated by focused ion beam milling (FIB) in an evaporated palladium microwire are presented. *In situ* atomic force microscopy (AFM) measurements proved that, in the presence of H₂, the trench closes and electrically connects the initially separated parts of the wire due to the increase in volume of the material. Therewith, an electrical current can be switched through the wire. With experiments under various H₂ concentrations and a mathematical model, we describe the closing mechanism of the trench with respect to various parameters, including the substrate material, film thickness, trench size and wire dimensions. Results have been compared with those from equivalent continuous wires. Thin SiO₂ and polyimide (PI) layers on silicon were used to study the effect of substrate elasticity. Sufficient lateral expansion of Pd to close trenches of up to 70 nm in width has only been observed on PI, which we attribute to its advantageous elastic properties. The scale of the response times allowed the observation of two superposing effects: the chemical conversion of Pd to PdH_x and the mechanical closing of the trench.

(Some figures in this article are in colour only in the electronic version)

1. Introduction

Hydrogen as a fuel is becoming of increasing interest as it constitutes an energy carrier which is absolutely free of polluting emissions. As it is highly explosive, flammable in the air and difficult to store, a variety of safety sensors are being developed for the reliable and continuous monitoring of hydrogen. The most prominent material for hydrogen detection by far is the transition metal palladium (Pd). Its outstanding ability to form a stable hydride (PdH_x), accompanied by large changes in its physical properties, has been the focus of intensive research over many years [1, 2].

The most straightforward and thus commonly used effect for hydrogen detection is the change in resistivity of palladium thin films [3, 4]. This effect has been explained by the increased scattering of electrons at interstitial states in the fcc lattice of palladium hydride which are occupied by hydrogen atoms. It leads to an increase in resistivity which is linearly dependent on the concentration of dissolved hydrogen in the

bulk up to atomic ratios of H/Pd \approx 0.7 [1, 2]. Other palladium-based sensing devices are based on optical fiber gratings [5], surface acoustic waves (SAWs) [6], Pd-coated cantilevers [7] or palladium-gate MOS junctions [8].

Favier *et al* [9] were the first to make use of the increase in material volume of palladium which occurs during the hydride formation process to close nanoscaled break junctions in electrodeposited palladium mesowires. It is well known that, with the absorption of hydrogen, the Pd to PdH_x transition induces a change in lattice constant of up to 3.5% [1]. In contrast to sensors based on Pd thin films, devices using such chemomechanical nanoswitches show an inverse behavior, namely a decrease in resistance in the presence of hydrogen. Response times as small as 20 ms have been reported [9, 10].

This nanogap approach was followed up by Kaltenpoth *et al* [11], who electrochemically deposited Pd nanoparticles into photolithographically defined channels in silicon, Luongo *et al* [12], who used porous silicon templates with a thin Pd film on the surface which showed an island-like structure with

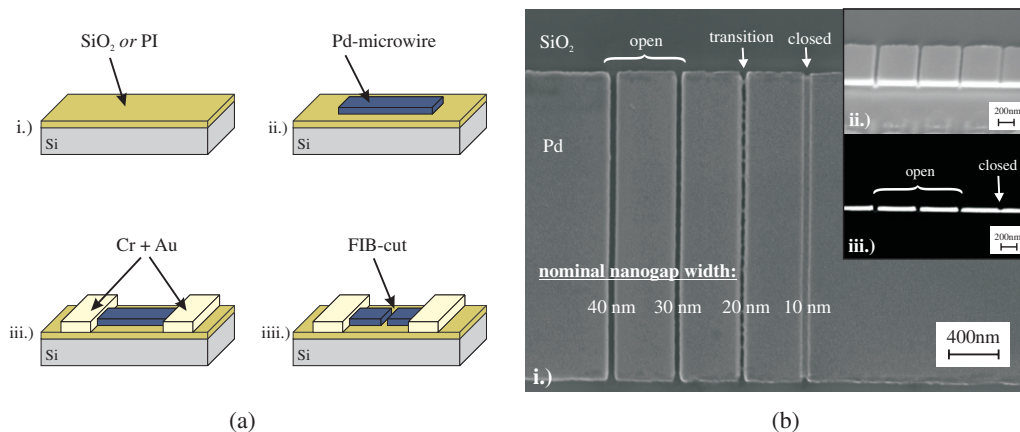


Figure 1. (a) Schematic process flow for fabrication of the sensing devices. Thermal SiO₂ (200 nm thickness) or spin-coated polyimide (2 μm thickness) was used as the intermediate layers. (b) Analysis of four exemplary nanotrenches by SEM. (i) FIB cuts (30 kV, 1 pA, total milling time 104 s) with different nominal widths (from left to right: 40, 30, 20, 10 nm) in a 50 nm thin Pd microwire and a 2.5 nm thin Ti adhesion layer on SiO₂, (ii) FIB milled cross section of the same trenches (with a thin carbon layer on top to avoid charging), (iii) the same image but with enhanced contrast. The images show open cuts, a partially open cut and a cut on the onset of milling. Redeposition and amorphization are visible as white shade along the trenches.

nanometer spaced metallic parts, and Kim *et al* [13], who made use of nanopores in anodized alumina templates for the electrodeposition of vertical Pd nanowires.

Dankert *et al* reported nanogap-based hydrogen sensors using ultrathin palladium films deposited by physical vapor deposition (PVD) which inherently showed statistically distributed metal islands only a few nanometers apart [14]. By extending this idea with the use of self-assembled monolayers between the substrate and the palladium layer, Xu *et al* fabricated a very fast and sensitive device which could detect 2% of H₂ within 70 ms [15].

The common feature shown by all these devices is the use of bottom-up approaches for the creation of self-organized nanogaps, whereas no *top-down* engineering approaches have been reported so far. A reliable, repeatable and scalable lithography-based fabrication method would enable the perfect control of the number and the geometrical arrangement of nanogaps between two electrodes, a high flexibility in the use of various deposition techniques, the choice of the most suitable substrate and an improved compatibility with system integration procedures. In particular, PVD methods such as evaporation, which are common techniques in microelectronics, enable the direct use of Pd on insulating substrates. Additional transfer processes as in the case of electrochemical methods can thus be avoided.

In this paper we present our investigation results on the use of a top-down approach for the fabrication of a hydrogen detector based on nanogaps in evaporated palladium. In particular, a focused ion beam (FIB), a well-known rapid prototyping nanofabrication tool, is used to mill a single nanotrench into a palladium microwire. We aim to examine the effect of the substrate, wire thickness and milling time on the final sensor characteristics. Continuous microwires were measured for comparison. The single trench approach turned out to be useful to study the switching mechanism and to model mechanical and electrical properties for the future design of top-down fabricated hydrogen sensors. Scaling-up to

a wafer scale for the parallel manufacturing of such prototyped devices could be imagined by technologies such as deep-UV or nanoimprint lithography (NIL) [16, 17].

2. Fabrication

2.1. Device fabrication

Palladium microwires were fabricated by e-beam evaporation at room temperature and a subsequent lift-off process (see figure 1(a)). The length of the wires is 85 μm with a width of 2.8 μm . Four different material thicknesses were chosen for a comparison, namely 10, 25, 50 and 100 nm. Experiments by RaviPrakash *et al* [4] with continuous palladium microwires prepared by sputtering have shown that the geometry of continuous wires has a negligible influence on the electronic signal under hydrogen. 100 nm thick Au electrode pads with a surface area of 1 mm² and a 10 nm thick Cr adhesion layer underneath were evaporated by shadow mask deposition, serving as electrical contacts. As substrates we used p-type silicon wafers onto which two different types of intermediate insulating layers were deposited: (i) a thermal wet oxide with a thickness of 200 nm as a rigid layer, and (ii) a 2 μm thick coating of polyimide (PI) as an elastic layer. The palladium wire was then either directly deposited by evaporation on top of it or by using an intermediate titanium (Ti) adhesion layer. The morphology of the thin films which were used was that of a densely packed film with an estimated grain size in the range between some few nanometers and 50 nm.

2.2. Creation of nanotrenches using FIB

For FIB milling, an FEI Nova 600 NanoLab FIB workstation was used. Besides its main applications, which are transmission electron microscopy (TEM) specimen preparation, microdevice editing and local deposition of materials, in recent

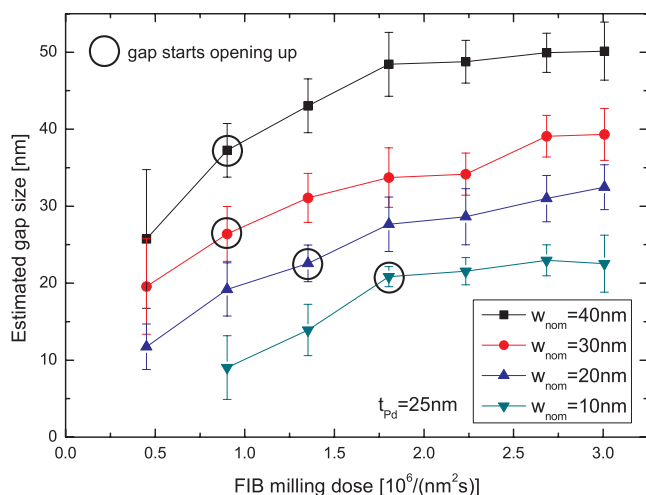


Figure 2. Estimated trench widths as a function of the FIB milling rate by SEM analysis (here, for a 25 nm thick Pd wire). The black circles indicate the threshold dose for milling, above which the trench is completely cut. For a thickness of 100 nm no open trenches were observed in the considered range of milling times. The error bars indicate variations and inaccuracies in the measurement of a single trench.

years the FIB has also proven to be a useful tool in the fabrication of nanoscaled devices [18–20].

A liquid metal ion source (LMIS) operated at 30 keV using Ga^+ ions and the smallest possible beam ($I = 1 \text{ pA}$) was used (nominal beam diameter 7 nm, dwell time 1 ms, overlap 50%). As redeposition limits the achievable aspect ratio and, especially at low dose levels, amorphization may induce the metal to swell [20], an initial test milling was performed. Trenches of four different nominal widths (10, 20, 30 and 40 nm) were milled into wires of various thicknesses using an intermediate SiO_2 layer and Ti adhesion films to find the optimum milling conditions. This was repeated on each of the wires for up to seven different milling times (figure 1(b)-i).

2.3. Characterization of nanotrenches

The width of the trenches was estimated using scanning electron microscopy (SEM). A typical result for the estimation of the trench sizes is shown in figure 2 for a 25 nm thick microwire. As shown in figure 1(b)-ii and (b)-iii, cross sectional profiles of the trenches created by the FIB, and an additional enhancement of the image contrast facilitated the evaluation of the milling dose where the trench opened up completely, when necessary. For higher doses, its width saturates at a value which is larger than the nominal width w_{nom} . Trenches with smaller nominal width showed a more pronounced redeposition. The typical minimum width where the trenches started to open up lay in the range of 20 nm for a wire of 25 nm thickness to 28 nm for a wire of 50 nm thickness. Corresponding threshold doses were in the range of $1\text{--}2 \text{ (nm}^2 \text{ s)}^{-1}$ and $1.7\text{--}2.7 \text{ (nm}^2 \text{ s)}^{-1}$, respectively. For the 10 nm thick wires, single beam milling (beam diameter: 7 nm) was used. Despite the low milling doses, the trench sizes were around 50 nm. The 100 nm thick wires could not be opened within the considered range for a trench width below 100 nm.

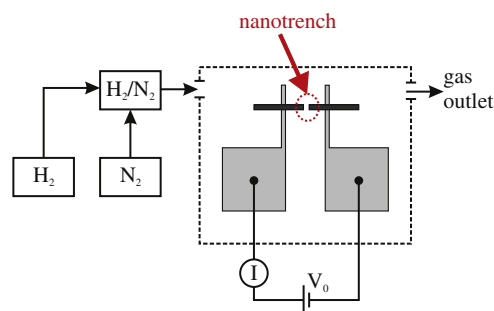


Figure 3. Schematic drawing of the measuring setup showing the microwire with contact pads which are placed inside a flow cell, electrical connections and the supply of the gases H_2 and N_2 .

Irregularities in the edge definition of the trenches are assumed to originate from interactions of impinging ions of the beam with the granular structure of the material. The Gaussian beam shape results in a variable trench width along its depth [21].

For electrical measurements under H_2 , single FIB cuts were performed using milling times above the threshold values. They would ideally be completely open in air ($I \approx 0 \text{ A}$) and possibly show a dependence on the hydrogen concentration caused by the observed slight variations in the trench geometry.

3. Experimental setup for hydrogen sensing

The measurements under hydrogen were performed using a fluidic flow cell made of polymethylmethacrylate comprising a compartment of dimensions $2 \text{ cm} \times 2 \text{ cm} \times 1 \text{ cm}$ which carries the chip. A dedicated gas line including four Bronkhorst flow meters was used for the regulation of H_2/N_2 mixtures between 0.5 and 100 vol% of hydrogen. A constant electric potential was provided by a PGSTAT12 potentiostat from Autolab which simultaneously measured the corresponding current through the device. Figure 3 shows a schematic of the setup.

4. Experimental results and discussion

4.1. Continuous microwires

The electrical transport behavior of discontinuous palladium films is known to be composed principally of two opposing effects [22]: the superposition of the change in contact area due to the narrowing of the discontinuities (in our case, the nanotrench) and the change in specific resistivity of the material due to the conversion of Pd to PdH_x . A schematic representation of both effects is given in figure 4(a). To distinguish between those effects, continuous palladium microwires with dimensions equal to the wires with nanotrenches were fabricated and electrically measured in H_2/N_2 mixtures. Typical signals for wires of various thicknesses at 4% H_2 are shown in figure 4(b).

The observed decrease in current and the response times in the range of several seconds up to about 100 s correspond to what has been reported in the literature [3, 4]. The response time decreases with both decreasing film thickness

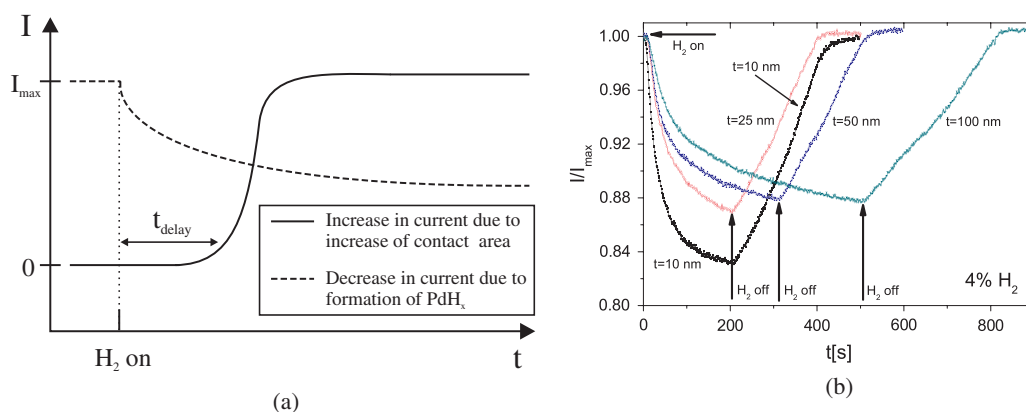


Figure 4. (a) Schematic representation of the two opposing effects which contribute to the change in current in a palladium microwire including a nanotrench on hydrogen exposure. The conversion from Pd to PdH_x results in a decrease in current whilst the mechanical narrowing and eventual closing of the nanotrench result in an increase of the current. Depending on the trench width, a time delay might be present. (b) Electrical response and recovery measurements with continuous microwires of various thicknesses t under hydrogen (4% H₂ in N₂, $V_0 = 1$ mV, room temperature).

and increasing H₂ concentration, due to a faster conversion process. In contrast, the recovery time decreases with both decreasing film thickness and decreasing H₂ concentrations, respectively.

4.2. Microwires with single nanotrenches on SiO₂

Microwires which were fabricated on SiO₂ without adhesion layers showed a very poor adhesion and peeled off after a few H₂/air cycles. This is caused by the high mechanical stress induced by the Pd to PdH_x conversion in the thin microwire which can be on the order of several GPa [23]. Samples using the same substrates but incorporating a thin Ti adhesion layer underneath the Pd wire did not show any closing effects even after H₂ exposure times as long as 500 s.

4.3. Microwires with single nanotrenches on PI

Pd microwires on PI underlayers, however, showed reversible switching under hydrogen. With a Young's modulus of approximately 8.5 GPa, PI is flexible and allows the metal to expand and contract in plane. While the 25 and 50 nm thick wires both showed trenches which closed under hydrogen, only minor closing effects could be observed with the wires of 10 nm thickness, even at concentrations as high as 100% H₂. Within such thin films, despite the advantageous mechanical properties of PI, the stress induced at the metal–polymer interface still does not relax sufficiently to allow a complete lattice expansion to close the trench [14, 23, 24]. Wires with a thickness of 100 nm were not completely cut by FIB for the considered trench widths due to the required high aspect ratio. Increasing nominal widths resulted in large trenches which could not close even at 100% H₂.

A typical electrical signal during H₂/air cycles at different concentrations is shown in figure 5(a) for a 25 nm thick Pd wire with a 1.5 nm thin Ti adhesion layer on PI (sample 1). The trench width for this sample was about 61 nm ± 5 nm. In air, no current is flowing since the gap remains open. A reversible H₂-dependent response to hydrogen is observed, however. The

Table 1. Delay times t_D , response times t_R and recovery times t_F for the electrical currents which were measured in figure 5(a) (sample 1, 25 nm thick wire).

$c(\text{H}_2)$ (%)	t_D (s)	t_R (90% I_{\max}) (s)	t_F (10% I_{\max}) (s)
20	7	54	370
10	35	142	375
5	53	304	326
4	74	362	303
3	115	498	300
2	221	—	—

signal amplitude which is proportional to the H₂ concentration is characteristic for a gradual opening and closing of the trench. The minimum detectable H₂ concentration of this sensor was 2%. The decrease in current amplitude for the third exposure to 10% H₂ in comparison to the first two peaks demonstrates the occurrence of an activation process, since irreversible changes in morphology of Pd occur during the very first exposures to H₂ [25].

The comparison of the maximum current through this sample with a corresponding continuous wire shows that only a part of the trench is actually closing. The maximum currents in the closed state are well below 1 μA, whereas the currents for the equivalent continuous wire range from 2 to 4 μA. These low and H₂-dependent values of the current confirm that the change in contact area of the trench is a gradual process, reflecting its shape and surface morphology. It should be mentioned that even a wire with a fully closed trench might not electrically behave exactly the same as an equivalent continuous wire. An additional contact resistance caused by the two touching interfaces is expected.

The values for the response times t_R and recovery times t_F , here defined respectively as 90% and 10% of the maximum current, are shown in table 1. t_R increases with decreasing hydrogen concentration due to a slower diffusion process at low H₂ surface pressures. t_F slightly decreases with decreasing H₂ concentration, which is due to the fact that less gas has to diffuse out of the material. The delay time t_D which was

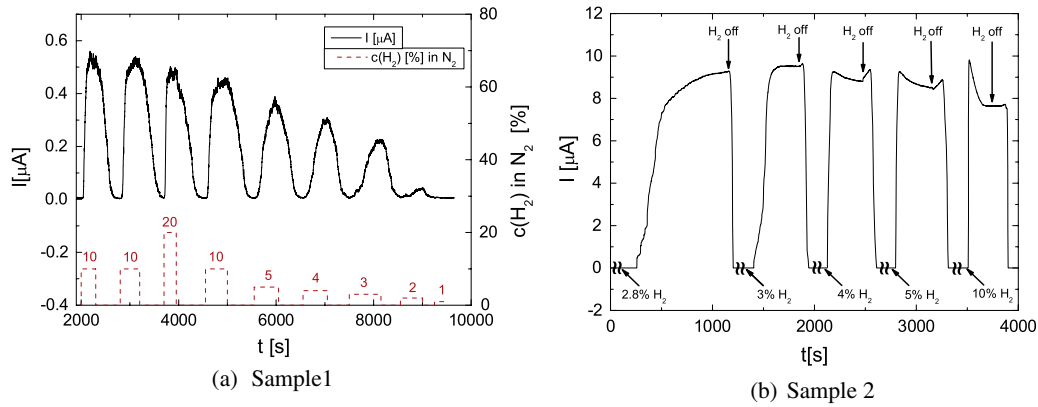


Figure 5. Electrical measurements of typical Pd microwires with a 1.5 nm thick adhesion layer on a 2 μm thick polyimide (PI) coating and a single nanotrench under various H_2 /air cycles (measured at room temperature, $V_0 = 20$ mV). (a) Sample 1: 25 nm thick Pd wire, trench width: 61 ± 5 nm. (b) Sample 2: 50 nm thick Pd wire, trench width: 26 ± 5 nm. The superposition of the mechanical closing of the gap (resulting in an increase in current) and the change in resistance due to the conversion of Pd to PdH_x (resulting in a decrease in current) become visible at H_2 concentrations above 3%. No response was observed for H_2 concentrations below 2.5%.

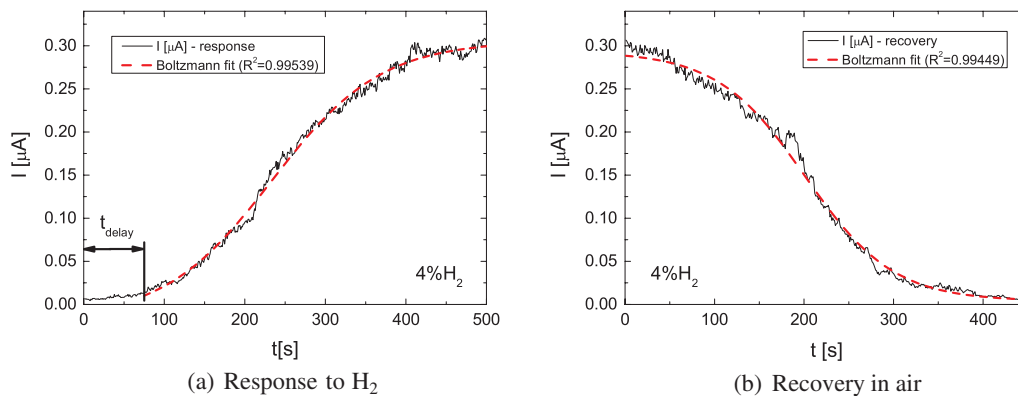


Figure 6. A typical example of fitting the sensor response and recovery currents by a Boltzmann function (25 nm thick Pd wire, 4% H_2).

observed at each response is associated with the long distance across the trench which has to be overcome before the first mechanical contact.

Numerical fitting of both the response (see figure 6(a)) and the recovery (see figure 6(b)) curves showed a good agreement with the Boltzmann function for concentrations between 2% and 20%:

$$I(t) = \alpha + \beta \left(1 + \exp \left[\frac{t - t_0}{\tau} \right] \right)^{-1} \quad (1)$$

where τ is the time constant of the signal, t_0 the time constant, β the amplitude and α the shift along the time axis.

However, these fits are only valid when the effect of hydride conversion in the signal is negligible. Since the delay times were as long as several tens of seconds, most of the conversion from Pd to PdH_x had already taken place before the mechanical closing came into effect. The Boltzmann sigmoidal fit thus seems to represent the gradual closing of the trench.

Samples which exhibited smaller gaps and therewith shorter delay times revealed the superposition of electrical and mechanical effects within the electrical signal. An example is shown in figure 5(b) in the case of a 50 nm thin Pd wire on PI (sample 2). The trench width was about

26 ± 5 nm. Upon hydrogen loading at higher concentrations (here, $\geq 3\%$ H_2), a fast increase followed by a minor decrease in current is observed. The mechanical closing effect is strongly pronounced in the signal since the effect of conversion to PdH_x is hidden during the initial delay. Further increasing of the H_2 concentration accentuates the effect of conversion, visible as a stronger drop in current. At low H_2 concentrations, thus long delay times, the visibility of the chemical contribution may not be apparent. This can for example be seen for the measurement at 2.8% H_2 . In contrast, at H_2 desorption the effect of chemical reconversion on the signal is faster in comparison with the mechanical opening. It hence shows an initial increase, followed by a sudden drop in current as soon as the two contact surfaces become detached.

As already observed with sample 1, the recovery times, unlike the response times, become shorter with decreasing H_2 concentrations. The recovery times are in both cases even undercutting the response times below certain H_2 concentrations. The longer recovery times for higher concentrations mainly seem to result from a delay in the mechanical relaxation of the material. This behavior could be a result of the interplay of different effects such as the previously mentioned decreasing out-diffusion time, the elastic relaxing of

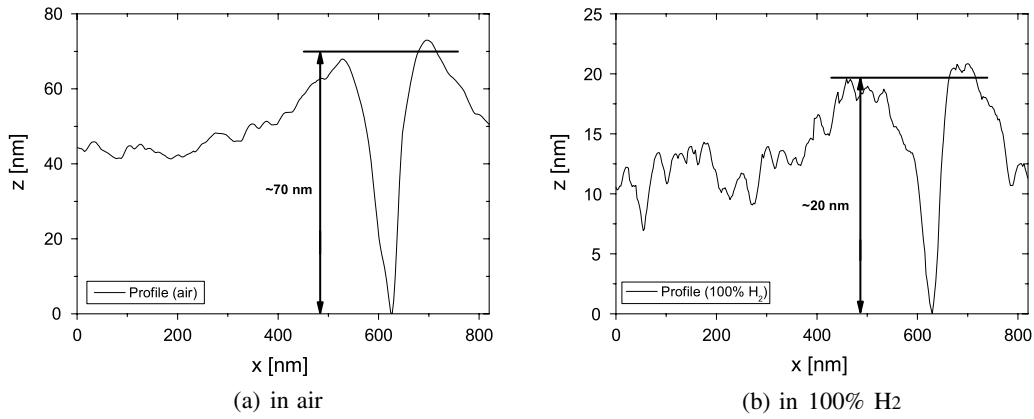


Figure 7. AFM profile of a nanotrench in a 50 nm thick Pd microwire in air (a) and hydrogen (b), respectively. The FIB cut is deeper than the thickness of the wire. At 100% H₂, approximately 30 nm of the total wire thickness is closed.

Table 2. Response times t_R and recovery times t_F for the electrical currents in figure 5(b). Due to the complex response signal, the response times given for concentrations higher than 3% are taken at the peak value of the signal (sample 2, 50 nm thick wire).

$c(\text{H}_2)$ (%)	t_D (s)	t_R (90% I_{\max}) (s)	t_F (10% I_{\max}) (s)
10	19	9 (peak)	160
5	34	33 (peak)	148
4	49	52 (peak)	122
3	50	149	73
2.8	202	406	46

the substrate and built-up stress in the contact zone which first has to decrease sufficiently before the two contact interfaces are able to detach. The values for the characteristic times of sample 2 are given in table 2.

The maximum current of about 9 μA through this sample under H₂ almost correspond to the values for an equivalent continuous wire. This is even the case for H₂ concentrations close to the switching threshold, which is close to 2.8% of H₂ (see figure 5(b)), and indicates a less gradual change in trench width as compared to sample 1.

Another result of the early saturation of the mechanical effect is the decrease in current in a final equilibrium state for increasing H₂ concentrations. A unique proportional dependence of the signal on the H₂ concentration thus only exists before saturation occurs.

4.4. AFM measurements under H₂

In situ AFM measurements were performed on a 50 nm thin Pd microwire on PI in order to confirm that mechanical closing occurs during hydrogen exposure. A typical trench profile of a gap which did not completely close under hydrogen is shown in figure 7. In this example, approximately 30 nm of the total trench height was closed at 100% of H₂.

4.5. Influence of material thickness

As already mentioned, another influence on the electrical signal is the thickness of the wire. First, the influence of

adhesion on the mechanical expansion decreases with the distance to the surface. The thicker the wire, the weaker the influence of the surface. Second, it determines the time needed for full hydride conversion (see figure 4(b)) and therewith the shape of the electrical signal. To explain this, we assume a constant mechanical contribution for different wire thicknesses. For thin wires, the hydride formation will occur on a faster timescale than the mechanical effect, being hidden in the response pulse. Meanwhile, for thicker wires, the hydride formation will occur on a longer timescale than the mechanical effect, shaping the response pulse in a visible way. As it was not possible to precisely keep the gap size constant with the current fabrication method, no experimental data can be given here.

5. Modeling

Based on the experimental results, we propose a simple model to describe the signals which were observed. Due to the good agreement with the Boltzmann function, the gradual mechanical closing mechanism is assumed to have a probabilistic nature. The trench is considered as many elementary switches arranged in parallel, with normally distributed threshold concentrations around a mean value μ_T and a standard deviation σ_T . In an open state, the resistance of such an elementary switch is infinitely high, whereas in a closed state it represents a resistor R_i with a H₂-dependent resistance. The total resistance of the trench R_T then simply is $R_T = (\sum_{i=1}^n 1/R_i)^{-1}$. The two separated halves of the wire are each resistors R_W which are dependent on the H₂ concentration in the bulk. A schematic model together with an SEM image of a real nanotrench is shown in figure 8.

The change in resistance for each R_i and R_W is described by an analytical model which has been developed by Pick *et al*, who examined H₂ absorption in Nb films [26]. Cabrera *et al* later used these analytical expressions to fit experimental data obtained with palladium thin films under H₂ exposure [3].

Based on these assumptions, the time-dependent current through the wire can be written as a series of R_W and R_T :

$$I(c_{\text{H}_2}, t) = V_0 \left(2R_W(c_{\text{H}_2}, t) + R_T(c_{\text{H}_2}, t) \right)^{-1} \quad (2)$$

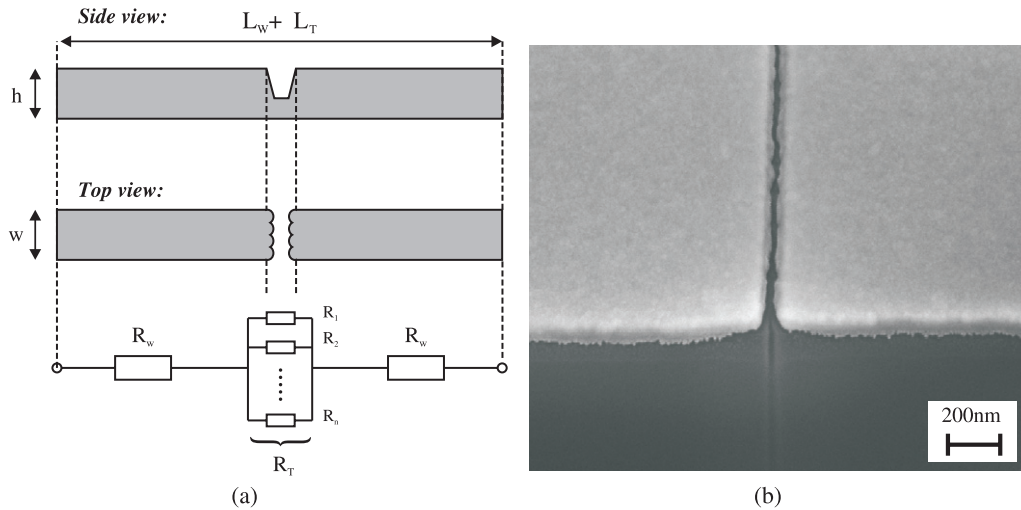


Figure 8. (a) Schematic of a microwire with a nanotrench, modeled as a series of resistors. R_T is the total resistance of the nanotrench and it consists of n resistors R_i arranged in parallel. The normally distributed threshold values describe the gradual closing of the gap with increasing H_2 concentrations. (b) SEM image of a part of a nanotrench in a 50 nm thin Pd microwire with a 1.5 nm thin titanium adhesion layer on polyimide (PI, dark area on the bottom).

where V_0 is the applied potential and c_{H_2} is the hydrogen concentration in the bulk. Splitting up the resistances into their geometrically dependent ($\Psi_{W/T} = L_{W/T}/(w \cdot h)$), and material-dependent ($\rho_0(c_{H_2}, t)$) parts, one obtains

$$I(c_{H_2}, t) = V_0 \left[\rho_0(1 + y(t)\gamma) \left(\frac{L_W}{w_W \cdot h_W} + \frac{L_T}{w_T \cdot h_T} \right) \right]^{-1} \quad (3)$$

where $y(t)$ the normalized atomic fraction x/x_{\max} of H in Pd depending on the time t , ρ_0 the specific resistance of Pd in air, and γ the linear factor describing the relative change in resistance with the atomic fraction of H in Pd, which is around 3.06 [1]. The function $y(t)$ is obtained by solving the analytic expression by Pick *et al* for a specific film thickness, H_2 concentration and time. The indices W and T denote dimensions referring to the wire or the trench, respectively.

Since the geometric contribution of the full wire, here referred to as Ψ_W , is known and constant, Ψ_T of the trench is dependent on the H_2 concentration and not known *a priori*. However, with the geometric dimensions of the wire and the width of the trench in air, the resistance of the trench in a fully closed state can be expressed as a fraction of the geometric contribution Ψ_W of the full wire. With the definition of a number n of elementary resistors along the trench, the geometrical contribution Ψ_i of a single resistor R_i can be calculated. Assuming a width of somewhat below 10 nm for each elementary contact across the trench, a value of $n = 400$ is arbitrarily chosen. The number of closed switches is then given by its product with the inverse H_2 -dependent integral of the normal distribution and equation (3) reads

$$I(c_{H_2}) = V_0 \left[\rho_0(1 + y(t)\gamma) \left(\Psi_W + \left(\int_0^{c_{H_2}(t)} f_N(\mu, \sigma) dx \right)^{-1} \frac{\Psi_i}{n} \right) \right]^{-1}. \quad (4)$$

The integral can now either be directly solved or a simple Monte Carlo algorithm can be used to simulate a ‘single experiment’.

The results show that considerable delay times may occur depending on the threshold values μ_T , the deviation σ_T , and the H_2 concentration. In figure 9(a), the typical sigmoidal shape of the response for low concentrations is shown for a 50 nm thick wire. At higher concentrations, the change in trench width saturates and the effect of conversion becomes visible. An initial, fast increase followed by a decrease in current is observed. This is in qualitative accordance with the experimental results in figure 5(b). The critical concentration for this effect can be determined by plotting the equilibrium values of the current against the H_2 concentrations as shown in figure 9(b).

5.1. Other influences

The model further suggests an influence of the dimensions of the wire. This is unlike the electrical response of a continuous wire, which shows no significant dependence on the geometry as experimentally shown by RaviPrakash *et al* [4]. The dependence of the normalized response signal on the length L_W of the wire in figure 10 shows that the response time becomes shorter for increasing L_W . For a wire of high resistance, the main contribution of R_T to the total resistance occurs only at the onset of closing as its relative influence strongly decreases with increasing number of closed elementary switches. In contrast, for a short wire the trench resistance R_T is dominant and the total current is governed by its gradual change over the full scale.

It has to be mentioned that experimental verification of these theoretical considerations with current fabrication and metrology methods is very difficult to obtain. An extremely precise knowledge and control of the gap size would be necessary in order to distinguish between effects which result from different gap sizes, morphologies, wire dimensions or H_2 concentrations.

Furthermore, surface adhesion, friction and elastic effects at the wire–substrate interface have an influence on the

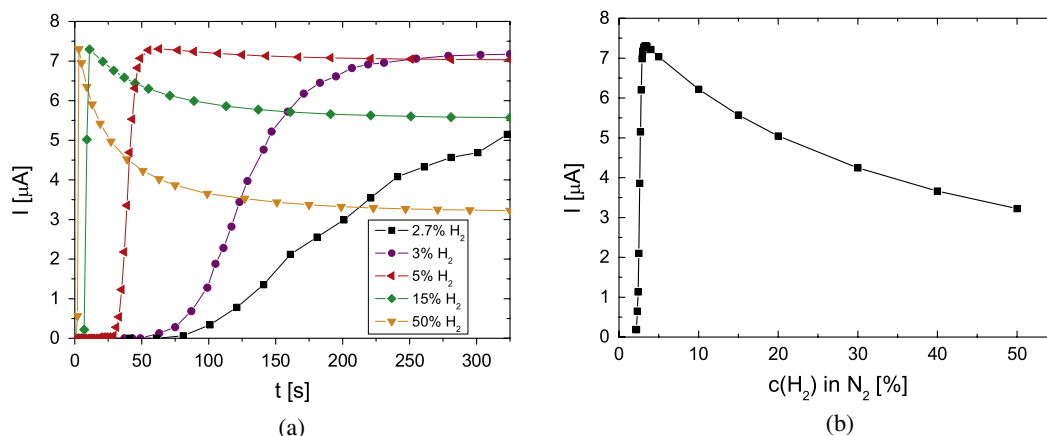


Figure 9. (a) Simulation result for the electrical response of a microwire to different H₂ concentrations in the bulk. The microwire has a length of $L_W = 100 \mu\text{m}$, a width of $w_W = 3 \mu\text{m}$ and a thickness of $h_W = 50 \text{ nm}$. The trench has a mean threshold concentration of $\mu_T = 0.04 \mu\text{m}$ with a standard deviation of $\sigma_T = 0.005$. (b) Simulation result of currents after 325 s for a microwire with a length of $L_W = 100 \mu\text{m}$, a width of $w_W = 3 \mu\text{m}$, and a thickness of $h_W = 50 \text{ nm}$. The trench has a mean threshold concentration of $\mu_T = 0.04 \mu\text{m}$ with a standard deviation of $\sigma_T = 0.005$. At $c_{\text{H}_2} \approx 3.3\%$, the conversion effect becomes dominant.

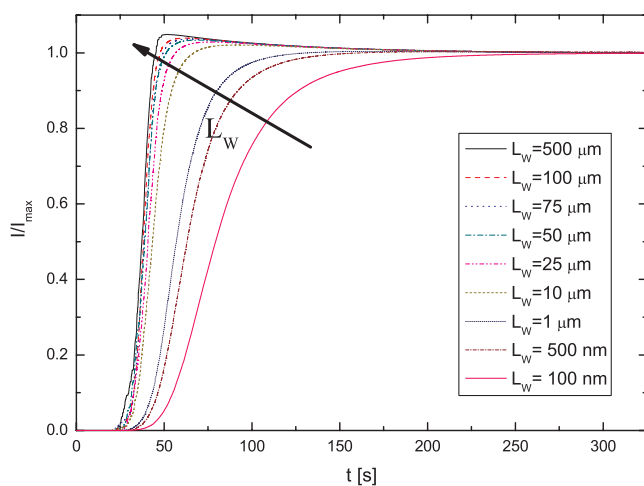


Figure 10. Normalized electrical response of a wire with a nanotrench for different theoretical lengths L_W of the wire. Longer wires show a faster overall response ($h_W = 50 \text{ nm}$, $\mu = 0.04$, $\sigma = 0.005$, H/Pd = 5%, $w_W = 3 \mu\text{m}$), $V_0 = 1 \text{ mV}$.

expansion mechanism. Since no experimental comparative data for various substrate materials are available, these effects have not yet been included in the model. An incorporation could be imagined by adding a mass–spring–damper model as a first approach.

6. Summary and conclusion

We have demonstrated a top-down approach for the fabrication of a nanotrench-based hydrogen sensor in a palladium thin film wire. Focused ion beam (FIB) milling was used to create a single nanotrench in microwires fabricated by e-beam evaporation. Measurements under hydrogen showed a reversible switching of an electrical current through the wire which was dependent on the hydrogen concentration. Elastic substrates such as polyimide allowed the metal

to expand sufficiently to close trenches of several tens of nanometers in width. The palladium wires required adhesion layers in order to support the stress created upon hydrogen loading. The influence of the film thickness is manifold: very thin films allow a fast diffusion of H₂ and enable the milling of narrow trenches. On the other hand, mechanical constraints given by the adhesion force between the metal and the polymer interface seem to impair the lateral expansion, especially at close distances to the surface.

The timescale of the sensor response allowed the observation and analysis of two superposing effects: the mechanical closing of the trench and the chemical conversion of Pd to PdH_x. The differences between the electrical signals which have been observed for various microwires are attributed to different trench widths and local variations, as well as the thickness of the wires.

A simple model based on the experimental results has been proposed to describe the electrical response of the wires. Besides the qualitative agreement with the experimental results it showed a dependence of the response time to the lateral geometrical extent of the wire which is unlike the behavior of continuous wires. A more precise and repeatable fabrication and eventually the comparison of the model and measurements would require *in situ* monitoring of the current through the wire while FIB milling [27]. This could greatly increase the precision of the final trench dimensions.

Acknowledgments

We would like to acknowledge the financial support from the FP6 Integrated Project HySYS SES6-019981, the Center of MicroNanotechnology (CMI) in Lausanne for technical consulting and support and Michel Ramonda from LPCP (Laboratoire de microscopie en champ proche), UM-II in Montpellier, for AFM measurements under hydrogen.

References

- [1] Lewis F A 1976 *The Palladium Hydrogen System* (New York: Academic)
- [2] Flanagan T B and Oates W A 1991 *Annu. Rev. Mater. Sci.* **21** 269
- [3] Cabrera A L and Aguayo-Soto R 1997 *Catal. Lett.* **45** 79
- [4] RaviPrakash J, McDaniel A H, Horn M, Pilione L, Sunal P, Messier R, McGrath R T and Schweighardt F K 2006 *Sensors Actuators B* **120** 439
- [5] Trouillet A, Marin E and Veillas C 2006 *Meas. Sci. Technol.* **17** 1124
- [6] D'Amico A, Palma A and Verona E 1982 *Appl. Phys. Lett.* **41** 300
- [7] Baselt D R, Fruhberger B, Klaassen E, Cemalovic S, Britton C L Jr, Patel S V, Mlsna T E, McCorkle D and Warmack B 2003 *Sensors Actuators B* **88** 120
- [8] Dwivedi D, Dwivedi R and Srivastava S K 2000 *Sensors Actuators B* **71** 161
- [9] Favier F, Walter E C, Zach M P, Benter T and Penner R M 2001 *Science* **293** 2227
- [10] Walter E C, Favier F and Penner R M 2002 *Anal. Chem.* **74** 1546
- [11] Kaltenpoth G, Schnabel P, Menke E, Walter E C, Grunze M and Penner R M 2003 *Anal. Chem.* **75** 4756
- [12] Luongo K, Sine A and Bhansali S 2005 *Sensors Actuators B* **111/112** 125
- [13] Kim K T, Sim S J and Cho S M 2006 *IEEE Sens. J.* **6** 509
- [14] Dankert O and Pundt A 2002 *Appl. Phys. Lett.* **81** 1618
- [15] Xu T, Zach M P, Xiao Z L, Rosenmann D, Welp U, Kwok W K and Crabtree G W 2005 *Appl. Phys. Lett.* **86** 203104
- [16] Ito T and Okazaki S 2000 *Nature* **406** 1027
- [17] Chou S Y, Krauss P R and Renstrom P J 1996 *J. Vac. Sci. Technol. B* **14** 4129
- [18] Matsui S and Ochiai Y 1996 *Nanotechnology* **7** 247
- [19] Reyntjens S and Puers R 2001 *J. Micromech. Microeng.* **11** 287
- [20] Tseng A A 2005 *Small* **10** 924
- [21] Vasile M J, Nassar R, Xie J and Guo H 1999 *Micron* **30** 235
- [22] Morris J E, Kiesow A, Hong M and Wu F 1996 *Int. J. Electron.* **81** 441
- [23] Laudahn U, Faehler S, Krebs H U, Pundt A, Bicker M, Huelsen U v, Geyer U and Kirchheim R 1999 *Appl. Phys. Lett.* **74** 647
- [24] Pundt A, Laudahn U, Huelsen U v, Geyer U, Wagner T, Getzlaff M, Bode M, Wiesendanger R and Kirchheim R 2000 *Mater. Res. Soc. Symp. Proc.* **594** 75
- [25] Frazier G and Glosser R 1980 *J. Less-Common. Met.* **74** 89
- [26] Pick M A, Devenport J W, Strongin M and Dienes G J 1979 *Phys. Rev. Lett.* **43** 286
- [27] Nagase T, Gamo K, Ueda R, Kubota T and Mashiko S 2006 *J. Microlith. Microfab. Microsyst.* **5** 011006